GEOPHYSICS, VOL. 46, NO. 8 (AUGUST 1981); P. 1137–1147, 14 FIGS.

GL04094

The telluric-magnetotelluric method in two- and three-dimensional environments

John A. Stodt*, Gerald W. Hohmann‡, and Sam C. Ting§

ABSTRACT

The assumption of spatial uniformity of the horizontal magnetic field, which is an implicit assumption made in straightforward applications of the telluric-magnetotelluric (T-MT) method, is not always valid near conductivity inhomogeneities. For a two-dimensional (2-D) case, the transverse electric mode horizontal magnetic field may vary more than a factor of three. The spatial variation of the horizontal magnetic field is not as great over three-dimensional (3-D) inhomogeneities, but it may still contribute significantly to impedance magnitude and phase over shallow inhomogeneities at higher frequencies.

Spatial variation of the horizontal magnetic field can cause T-MT impedances to differ significantly from magnetotelluric (MT) impedances. Consequently, MT modeling of T-MT field data could result in a misleading interpretation of conductivity structure. To avoid erroneous interpretation, numerical modeling programs should calculate actual T-MT responses, rather than MT responses, for comparison with T-MT data. Resolution of a conductivity structure which produces significant spatial variation of the magnetic field is less with T-MT data than with an equal number of MT data. However, the increased number of data obtained from a T-MT survey may offset this shortcoming if the data are properly interpreted.

INTRODUCTION

A telluric-magnetotelluric (T-MT) survey differs from a conventional magnetotelluric (MT) survey in that MT data (magnetic and electric field data) are collected only at selected base stations, with telluric data (electric field data) being collected at a number of remote sites in the vicinity of each base station, as shown in Figure 1. Telluric field measurements at a remote site are recorded simultaneously with either the magnetic or telluric field measurements at the nearest base site. If the base station magnetic fields are utilized, and standard techniques for obtaining impedance estimates from field data (e.g., Hermance, 1973) are applied to the simultaneously recorded base station magnetic and remote station electric field components, an approximation to the MT impedance tensor at the remote site is obtained. Alternatively, a telluric transfer tensor relating simultaneously recorded telluric fields at the base and remote sites may be estimated. The product of the telluric transfer tensor estimate and the base station MT impedance tensor estimate then yields the same approximation to the MT impedance tensor at the remote site as the first calculation does, except for differences due to different noise contents of the respective data sets. It is obvious that the degree of approximation is a function of how uniform the horizontal magnetic field is between the base and remote sites. If the magnetic field is spatially uniform, then the T-MT transfer impedance tensor equals the MT impedance tensor at the remote site.

Examination of the reflection coefficients at the surface of a one-dimensional (1-D) earth for representative earth parameters shows that a plane-wave source of arbitrary incidence produces horizontal magnetic and electric fields which are nearly uniform laterally. Further, the reflection coefficients show that only the electric field depends upon the conductivity structure, while the magnetic field is very nearly twice the incident field and is independent of the conductivity structure. These observations led Cagniard (1953) to suggest using a scalar T-MT method to obtain offshore 1-D MT soundings, by making onshore magnetic field measurements simultaneously with offshore telluric field measurements. Yungul (1966) suggested that scalar T-MT surveys could also be used to obtain correct two-dimensional (2-D) TM

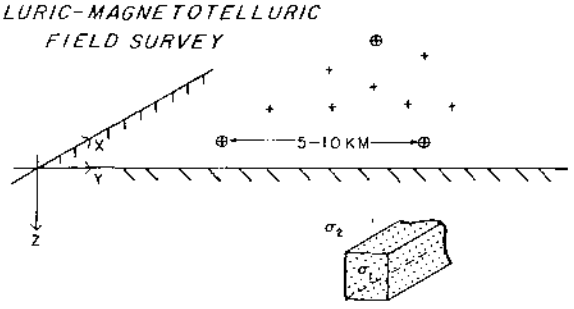

FIG. 1. T-MT survey field procedure. Circled crosses denote MT base stations; crosses denote remote telluric sites.

Presented at the 48th Annual International SEG Meeting November 1, 1978, in San Francisco. Manuscript received by the Editor October 4, 1979; revised manuscript received December 29, 1980.
*University of Utah Research Institute, Earth Science Laboratory, 420 Chipeta Way, Suite 120, Salt Lake City, UT 84108.
‡Department of Geology and Geophysics, University of Utah, Salt Lake City, UT 84112.
§Mobil Research and Development, Field Research Lab., P.O. Box 900, Dallas, TX 75221.

mode impedance estimates if the strike direction were known, and to obtain correct 1-D impedances when the base and remote site layered structure differed, provided both sites were sufficiently remote from transition zones where the conductivity structure was multidimensional. He also pointed out that simultaneous electric field measurements at the base and remote sites were sufficient to construct impedance estimates at the remote site, once the base station impedances were known. Finally, Hermance and Thayer (1975) suggested that tensor T-MT measurements could be used to estimate the remote site MT impedance tensors over multidimensional conductivity structures, provided the magnetic field was essentially laterally uniform. However, they did not provide a quantitative assessment of the validity of assuming a laterally uniform magnetic field, or of the effect of spatial variation in the magnetic field on the T-MT impedance estimates.

The assumption that the magnetic field is laterally uniform has been made both when making theoretical calculations (e.g., Weaver, 1963; Geyer, 1972) and to expedite field studies (e.g., Swift, 1967; Hermance et al, 1976). Swift (1967, 1971), however, recognized the possibility of spatial variation of the horizontal 2-D TE-mode magnetic field and provided for it in his numerical calculations. He and others have documented spatial variations of this field component over simple 2-D structures. In particular, Hughes (1974) presented 2-D TE-mode calculations for a suite of frequencies and showed a spatial variation of nearly a factor of four in the horizontal magnetic field at 1 Hz over a simple basin model.

Jones (1973) provided a summary of early numerical and analog model studies of induction near conductivity inhomogeneities, with an extensive list of references. At that time, preliminary three-dimensional (3-D) finite-difference modeling calculations (Jones and Pascoe, 1972; Lines and Jones, 1973a, b) showed significant spatial variation in both horizontal magnetic field components near 3-D inhomogeneities. Wiedelt (1975) presented a 3-D integral equation solution and showed the spatial variation of the field components over a conductive prism model. He also illustrated the changes in behavior of E_x, H_y, and H_z (the 2-D TE-mode field components) as the strike-length of a conductive prism increased. However, his results were all presented at a single frequency.

The T-MT method is appealing because it saves time if magnetic field measurements are required at only a few selected sites. However, the horizontal magnetic field must be nearly uniform laterally for the T-MT transfer impedance tensor to represent accurately the MT impedance tensor at the remote site. Published modeling calculations which document spatial variation of the horizontal magnetic field follow no systematic format, and only limited 3-D results are available. It is therefore difficult to assess systematically and quantitatively from published data the importance of the spatial variation of the horizontal magnetic field over 2-D and 3-D inhomogeneities, or its effect on T-MT transfer impedance calculations. We provide a systematic study of the spatial variation of the horizontal electric and magnetic field components over some simple 2-D and 3-D structures. The general applicability of the T-MT method can be assessed once the differences in spatial behavior of electric and magnetic field components, as well as the difference in field behavior due to 2-D or 3-D structure, are understood. The modeling calculations also allow quantitative assessment of the effect of spatial variation in the magnetic field on T-MT data, because the T-MT transfer impedance tensor is the product of the remote site MT impedance tensor and a magnetic transfer tensor which linearly relates the horizontal magnetic field components at a base and remote site.

THEORY

We begin by separating the total electric and magnetic fields into the sum of a primary part (subscript p) equal to the MT response over a 1-D structure and a secondary part (subscript s) due to 2-D or 3-D electrical inhomogeneities. Maxwell's equations for the total fields are

$$\nabla \times \mathbf{E} = -z\mathbf{H},$$

and (1)

$$\nabla \times \mathbf{H} = y\mathbf{E},$$

where $z = j\omega\mu$, $y = \sigma + j\omega\varepsilon$, and $e^{+j\omega t}$ time dependence is assumed. Here, ω is radian frequency and μ, ε, and σ are permeability, permittivity, and conductivity, respectively, at each field point. We assume that the electrical parameters are linear, isotropic, and time independent at each field point. The assumption of linearity allows the coefficients z and y to be separated into sums of secondary (z_s, y_s) and primary (z_p, y_p) parts, representing the superposition of 2-D or 3-D electrical inhomogeneities on a background layered structure. Substituting the expressions

$$\begin{aligned} \mathbf{E} &= \mathbf{E}_p + \mathbf{E}_s, \\ \mathbf{H} &= \mathbf{H}_p + \mathbf{H}_s, \\ z &= z_p + z_s, \end{aligned} \tag{2}$$

and

$$y = y_p + y_s$$

into equations (1) and subtracting the primary field relations

$$\nabla \times \mathbf{E}_p = -z_p\mathbf{H}_p,$$

and

$$\nabla \times \mathbf{H}_p = y_p\mathbf{E}_p, \tag{3}$$

gives the secondary field equations

$$\nabla \times \mathbf{E}_s = -z_p\mathbf{H}_s - z_s\mathbf{H},$$

and

$$\nabla \times \mathbf{H}_s = y_p\mathbf{E}_s + y_s\mathbf{E}. \tag{4}$$

The terms on the far right of equations (4) can be treated as magnetic and electric sources for the secondary fields. If μ and ε are constant, the only source term present is $\sigma_s\mathbf{E}$, which represents a scattering current existing only in conductivity inhomogeneities. The fields associated with the scattering current propagate through the primary layered structure to produce the secondary fields observed at the earth's surface; we do not generally expect the secondary fields to be spatially uniform close to conductivity inhomogeneities. The relative magnitudes of the laterally uniform primary field components, compared to the secondary field contributions, then determine the lateral variation of the total fields at the earth's surface. We may establish some useful conclusions about the spatial behavior of the total magnetic field at the earth's surface from direct examination of equations (1).

Maxwell's equations decouple into two independent sets of equations for a 2-D structure excited by a plane wave source when the x-y coordinate axes coincide with the principal directions, defined parallel and perpendicular to strike, as in Figure 1. One set governs the behavior of E_x, H_y, and H_z and is referred to as the transverse electric or TE mode, while the other set governs the behavior of H_x, E_y, and E_z and is referred to as the transverse magnetic or TM mode. Mode identification is determined by the single component of electric or magnetic field for each mode which is transverse to the plane of incidence--the y-z plane in Figure 1.

The equations governing the TM-mode field components are

$$\frac{\partial E_z}{\partial y} - \frac{\partial E_y}{\partial z} = -zH_x,$$

$$\frac{\partial H_x}{\partial z} = yE_y, \tag{5}$$

and

$$-\frac{\partial H_x}{\partial y} = yE_z.$$

The last of equations (5) shows that the spatial variation of the TM-mode horizontal magnetic field depends upon the vertical component of total current density yE_z. At MT frequencies, the magnetic fields associated with displacement currents may be ignored when compared with those caused by conduction currents for realistic earth electrical structures. Because the conductivity of air is negligible, y_{air} is approximately zero, requiring an unrealistically large normal component of electric field above the air-earth interface to produce a significant conduction current density normal to the interface. Hence, from equation (5), the TM-mode magnetic field is nearly uniform laterally (see, e.g., d'Erceville and Kunetz, 1962) at a flat air-earth interface. A flat interface is assumed in subsequent discussions.

The equations governing the TE mode field components are

$$\frac{\partial H_z}{\partial y} - \frac{\partial H_y}{\partial z} = yE_x,$$

$$\frac{\partial E_x}{\partial z} = -zH_y, \tag{6}$$

and

$$\frac{\partial E_x}{\partial y} = zH_z.$$

Some researchers have imposed constant boundary conditions on particular TE-mode field components at the air-earth interface when solving for the field behavior over 2-D inhomogeneities (see, e.g., Neves, 1957; Weaver, 1963; Geyer, 1972). However, when the secondary fields E_s and H_s produced by conductivity inhomogeneities are significant, equations (6) allow no a priori conclusions to be drawn about the spatial behavior of individual TE-mode field components at the air-earth interface. Swift (1967, 1971) recognized that any spatial variations in the field components at the interface are smoothed out above it because the fields approximately obey Laplace's equation in the air. He incorporated a constant vertical current (H_y constant) boundary condition at the top of a sufficiently thick air layer when modeling the TE-mode with a 2-D transmission surface analogy.

Maxwell's equations for a 3-D structure excited by a plane-wave source do not generally decouple. However, since the normal component of total current density at the earth's surface is negligible for realistic conductivity structures at MT frequencies, we can write $(\nabla \times \mathbf{H})_z = yE_z = 0$. From this relation we find that

$$\frac{\partial H_y}{\partial x} = \frac{\partial H_x}{\partial y}. \tag{7}$$

Equation (7) partially constrains the spatial behavior of the horizontal magnetic field components, but it does not help in predicting the actual spatial variation of these fields from one point to another.

Equations (6) and (7) allow the possibility of spatial variation in the horizontal magnetic field at the earth's surface, for the 2-D TE mode and the 3-D case, respectively. Equations (4) suggest that such behavior is not only possible, but probable, provided the secondary source $y_s\mathbf{E}$ produces secondary fields comparable to the primary fields at the air-earth interface. We now assess the effects of such variation on the T-MT transfer impedance calculations. The MT equation relating base station horizontal electric and magnetic fields is

$$\begin{bmatrix} E_x^b \\ E_y^b \end{bmatrix} = \begin{bmatrix} Z_{xx}^b & Z_{xy}^b \\ Z_{yx}^b & Z_{yy}^b \end{bmatrix} \begin{bmatrix} H_x^b \\ H_y^b \end{bmatrix},$$

or, more compactly

$$\mathbf{E}^b = [\mathbf{Z}^b]\mathbf{H}^b. \tag{8}$$

Using the notation of Hermance and Thayer (1975), some additional relations may be written for the electric field at a remote station:

$$\mathbf{E}^r = [\mathbf{Z}^r]\mathbf{H}^r, \tag{9}$$

and

$$\mathbf{E}^r = [\mathbf{T}]\mathbf{E}^b. \tag{10}$$

Superscripts b and r refer to base and remote station measurements, respectively, and $[\mathbf{T}]$ is the telluric transfer tensor relating the horizontal electric fields at a base station to those at a remote station. d'Erceville and Kunetz (1962) recognized the existence of the linear relation in equation (10). Its validity is established heuristically by recognizing that the horizontal electric or magnetic field will at most suffer a change in amplitude, phase, and direction in response to a variable source or conductivity structure as we move from point to point at the earth's surface. Relation (10) describes such a change if the elements of $[\mathbf{T}]$ are complex. In addition, the elements of $[\mathbf{T}]$ will be time invariant if the source field structure is identical at the base and remote site. In this case, $[\mathbf{T}]$ measures only differences in electrical structure between the base and remote sites. Substituting equation (8) into equation (10) gives

$$\mathbf{E}^r = [\mathbf{T}][\mathbf{Z}^b]\mathbf{H}^b = [\mathbf{W}]\mathbf{H}^b. \tag{11}$$

Equation (11) defines the transfer impedance tensor $[\mathbf{W}]$ relating base station magnetic fields to remote station electric fields. In a calculation with field data, $[\mathbf{W}]$ is used as the impedance tensor at the remote telluric sites.

Hermance and Thayer (1975) assume that the horizontal magnetic field is approximately uniform spatially and accept $[\mathbf{W}]$ as an estimate of $[\mathbf{Z}^r]$. But, as the model studies of the next section verify, spatial uniformity of the horizontal magnetic field cannot always be expected in the vicinity of conductivity inhomogeneities. Hence, to evaluate the T-MT method, we need to examine the differences between $[\mathbf{W}]$ and $[\mathbf{Z}^r]$. By analogy with equation (10), we define a magnetic transfer tensor $[\mathbf{M}]$, relating the tangential magnetic fields at the base and remote sites:

$$\mathbf{H}^r = [\mathbf{M}]\mathbf{H}^b. \tag{12}$$

In general, $[\mathbf{M}]$ has the form:

$$[\mathbf{M}] = \begin{bmatrix} 1 + r_{xx} & r_{xy} \\ r_{yx} & 1 + r_{yy} \end{bmatrix}, \tag{13}$$

where the r_{ij} are unknown and possibly complex. Notice that $[\mathbf{M}]$ reduces to the identity matrix when $\mathbf{H}^r = \mathbf{H}^b$. Equation (12) is substituted into equation (9) to obtain an alternate expression for $[\mathbf{W}]$:

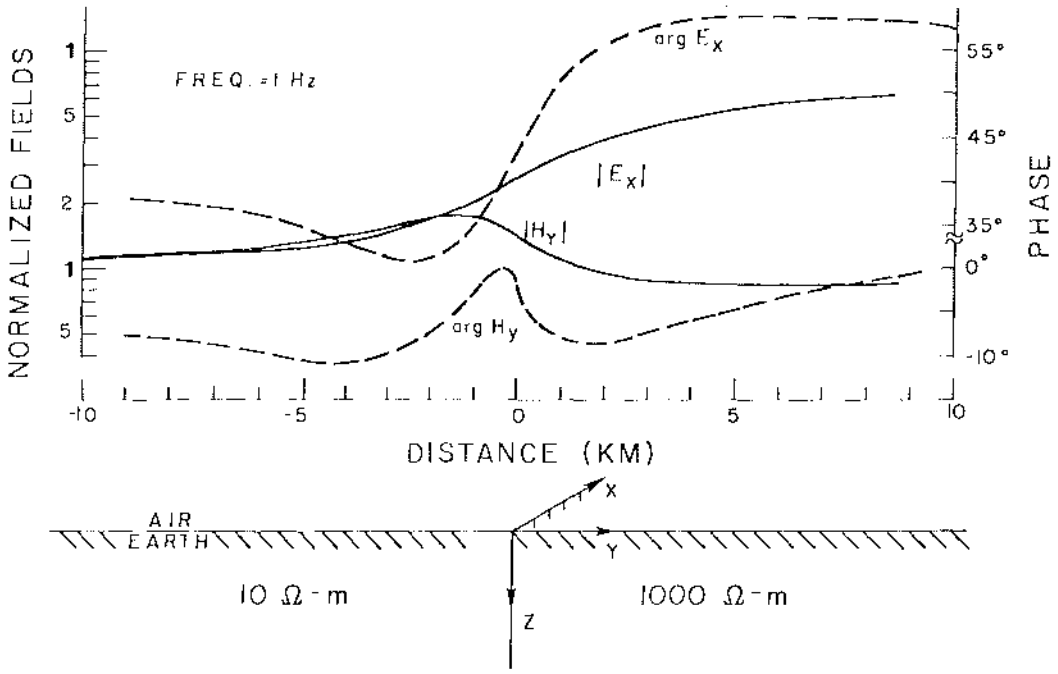

FIG. 2. Spatial variation of TE-mode horizontal field components across a 2-D vertical contact at 1 Hz. Arg E_x and arg H_y are phases of the respective components, while $|E_x|$ and $|H_y|$ are magnitudes of these components.

$$\mathbf{E}^r = [\mathbf{Z}^r][\mathbf{M}]\mathbf{H}^b = [\mathbf{W}]\mathbf{H}^b. \tag{14}$$

We cannot recover $[\mathbf{Z}^r]$ from $[\mathbf{W}]$ at a remote site, if $[\mathbf{M}]$ is not an identity matrix. To calculate $[\mathbf{M}]$ directly would require a simultaneous measurement of the magnetic fields at the base and remote stations, implying a full MT survey, which we wish to eliminate with the T-MT method. Equation (14) defines explicitly the difference between the remote site impedance tensor $[\mathbf{Z}^r]$ and the transfer impedance tensor $[\mathbf{W}]$. If $[\mathbf{W}]$ is rotated into new coordinates (x', y'), then

$$\mathbf{E}^{r'} = [\mathbf{P}]\mathbf{E}^r,$$
$$\mathbf{H}^{b'} = [\mathbf{P}]\mathbf{H}^b,$$

and

$$[\mathbf{W}'] = [\mathbf{P}][\mathbf{W}][\mathbf{P}^{-1}] = [\mathbf{P}][\mathbf{Z}^r][\mathbf{P}^{-1}][\mathbf{P}][\mathbf{M}][\mathbf{P}^{-1}], \tag{15}$$

where $[\mathbf{P}]$ is the usual orthonormal rotation matrix. Obviously, if $[\mathbf{M}]$ is not an identity matrix, then the principal directions determined from $[\mathbf{W}']$ will not in general agree with those determined from $[\mathbf{Z}^{r'}]$.

Both the MT impedance tensor $[\mathbf{Z}]$ and the magnetic transfer tensor $[\mathbf{M}]$ diagonalize in the 2-D case when a coordinate axis coincides with the strike direction, a consequence of mode separation. Then $[\mathbf{M}]$ has the form

$$[\mathbf{M}] = \begin{bmatrix} 1 & 0 \\ 0 & 1 + r_{yy} \end{bmatrix}, \tag{16}$$

where x is the strike direction. The expression for $[\mathbf{W}]$ becomes

$$[\mathbf{W}] = \begin{bmatrix} 0 & Z^r_{xy}(1 + r_{yy}) \\ Z^r_{yx} & 0 \end{bmatrix}, \tag{17}$$

showing that the transfer impedance tensor $[\mathbf{W}]$ still diagonalizes when rotated into the principal directions. Notice that Z^r_{yx}, the TM-mode MT impedance, is recovered at the remote site, but that W_{xy}, the TE-mode T-MT transfer impedance, will differ from Z^r_{xy} when H_y varies significantly. It is again obvious that we cannot recover Z^r_{xy} from $[\mathbf{W}]$ if $[\mathbf{M}]$ is not an identity matrix.

MODEL STUDIES

Numerical calculations over some simple 2-D and 3-D structures have been obtained using computer programs developed at the University of Utah. The 2-D results were calculated with a finite-element program originally developed by Rijo (1977), and subsequently modified by Stodt (1978). The 3-D results were calculated using an integral equation solution recently developed by Ting and Hohmann (1981).

Spatial variation of the horizontal field components along profiles in the symmetry planes of some simple 2-D and 3-D earth models is presented in Figures 2, 4, 6, 8, 9, 10, 13, and 14. The phases of the field components are plotted on a linear scale. The magnitudes are plotted on a logarithmic scale after normalization by the distant field, to allow direct assessment of the relative spatial variation in the magnitudes of the field components. For example, a factor of two difference in normalized magnitude between any two points along a profile produces the same vertical deflection on the graph regardless of the normalization constant.

For a 2-D earth, the ratio of remote site TE-mode T-MT and MT apparent resistivity estimates ($\rho_a = |E_x|^2/\omega\mu|H_y|^2$) due to spatial variation in the magnitude of H_y is just

$$|M_{22}|^2 = |1 + r_{yy}|^2 = |H^r_y|^2/|H^b_y|^2. \tag{18}$$

The ratio of the magnitudes of H_y at a base and remote site can be obtained directly from the graphs. Note that ρ_a varies as the ratio of the magnitudes of these fields squared. Equation (18) is not always valid for the 3-D case because mode separation does not usu-

ally occur, and hence the impedance tensor usually will not diagonalize for any orientation of coordinate axes. Then the impedance elements can no longer be obtained from ratios of orthogonal electric and magnetic field components in the principal directions, and the ratio $|H_y^r|/|H_y^b|$ in equation (18) must be replaced by either $|W_{xy}|/|Z_{xy}^r|$ or $|W_{yx}|/|Z_{yx}^r|$ when calculating the difference between T-MT and MT apparent resistivities.

Fortunately, any impedance tensor on a profile in a vertical symmetry plane of any 3-D prism model considered here still diagonalizes when the measurement axes are parallel to the unit normal vectors of the symmetry planes. In addition, the maximum deviation in the magnitude of the horizontal magnetic field from its background value occurs at the intersection of the vertical symmetry planes regardless of incident field polarization. Therefore, the maximum variation between MT and T-MT apparent resistivities observed in these symmetry planes may still be calculated by direct application of equation (18).

Two-dimensional results

The spatial variation of both magnitudes and phases of the TE-mode horizontal field components across a vertical contact with a 100:1 resistivity contrast is shown in Figure 2. This variation has been plotted for quarter-space resistivities of 10 and 1000 Ω-m at a frequency of 1 Hz. The magnitude of H_y can vary by a factor of two, while the phase of H_y can vary by ten degrees over a distance of 5 km.

The effect on T-MT apparent resistivities is shown in Figure 3. The solid line is the TE-mode MT apparent resistivity curve obtained from the finite-element solution. The curves plotted with the different symbols are T-MT apparent resistivities obtained using magnetic fields at the base station locations indicated by the appropriate symbols at the bottom of the graph. The base station spacing is 10 km, so that electric fields within 5 km of a particular base station are used with magnetic fields at that base station to calculate the T-MT apparent resistivities. More than a factor of three difference between T-MT and MT apparent resistivities occurs with this base station spacing. Notice that a shift of base station location of 2 km, from the circle symbol to the box symbol sites, causes significant variation in the T-MT apparent resistivities.

The spatial behavior of the fields as a function of frequency or resistivity, for a fixed resistivity contrast, can be predicted for the quarter-space model from data over one resistivity model at a single frequency by invoking electrodynamic similitude (Stratton, 1941, p. 488–490). When displacement currents are ignored, the condition of similitude requires that the characteristic number,

$$C = \omega\mu\sigma l^2, \tag{19}$$

be invariant at each field point to scale changes in the parameters (Cagniard, 1953; d'Erceville and Kunetz, 1962). Here, l represents a length scaling applied to all linear dimensions. For the quarter-space model we scale the abscissa in Figure 2 by the change in dimension scale factor l required to preserve invariance of C when frequency is varied or the resistivities are scaled. The spatial variation of the fields in any 5-km interval along the profile is less as frequency is decreased or as resistivities of the quarter-spaces are increased because the distance scale must be expanded to keep C constant. Similarly, the prism model results, given in this paper for specific frequencies, resistivities, and length scaling, apply for any combination of frequency, resistivity, and length scaling which preserves invariance of C at each field point.

Figure 4 shows the spatial variation in the TE-mode horizontal field components at three frequencies over a conductive prism of infinite strike-length and of width (1 km) equal to its depth of

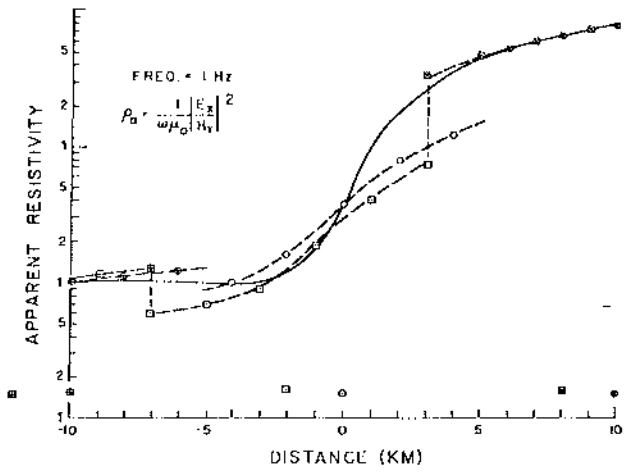

FIG. 3. Comparison of MT and T-MT apparent resistivities calculated from Figure 2. The solid line is the TE-mode MT apparent resistivity curve, while the dashed lines connecting the circle and box symbols are T-MT apparent resistivity curves calculated by using magnetic fields at the location of the corresponding symbol at the bottom of the graph.

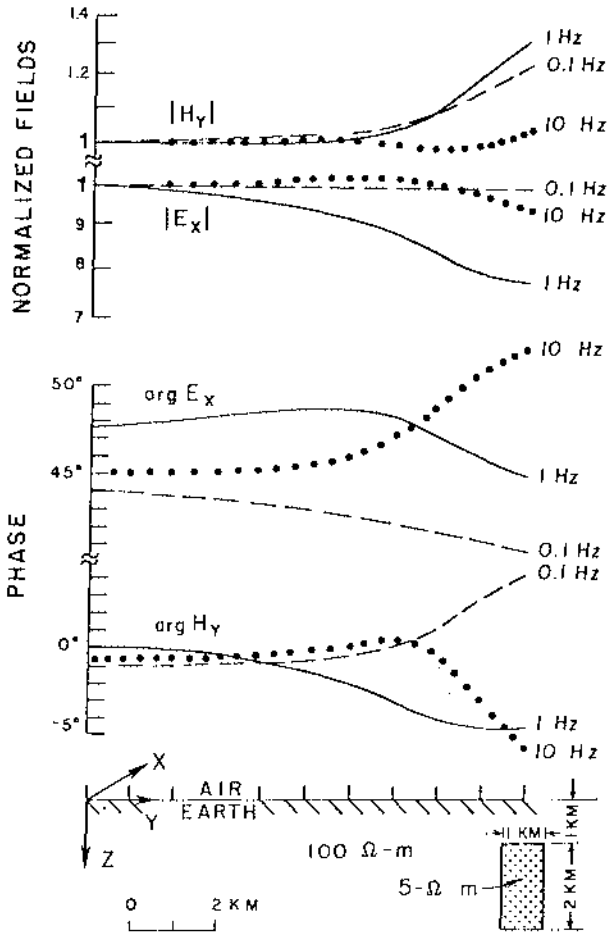

FIG. 4. Spatial variation of the TE mode horizontal field components across a deep 2 D prism.

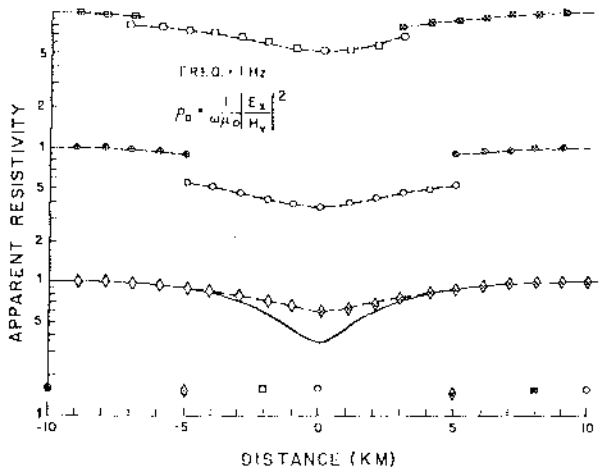

FIG. 5. Comparison of MT and T-MT apparent resistivities calculated from Figure 4. The solid line is the TE-mode MT apparent resistivity curve, while the dashed lines connecting the diamond, circle, and box symbols are T-MT apparent resistivity curves calculated by using magnetic fields at the location of the corresponding symbol at the bottom of the graph. Curves connecting the circle and box symbols have been shifted vertically for clarity.

burial. The resistivity contrast is 20:1, and the depth extent of the prism is twice its width. Only half of the profile has been plotted because of the obvious symmetry. It is apparent that the spatial variation in the horizontal magnetic field can contribute significantly to variations from background values of both apparent resistivity and impedance phase ($\phi = \arg E_x - \arg H_y$). In Figure 4, at 10 and 1 Hz, the spatial variation of the magnetic field contributes about equally with the spatial variation of the TE-mode electric field in the calculation of ρ_a and ϕ. As frequency decreases, spatial variation in the magnetic field becomes relatively more important. At 0.1 Hz and below, it accounts for nearly all of the observed spatial variation in apparent resistivity. The spatial variation of the TE-mode electric field over this model is relatively unimportant at low frequencies.

T-MT apparent resistivities were calculated from Figure 4 at 1 Hz for a number of base station locations. The results are plotted in Figure 5. The shapes of the T-MT apparent resistivity curves and their maximum anomalous responses depend significantly on the locations of the base stations.

Figure 6 shows the spatial variation of the TE-mode horizontal fields at four frequencies over a prism of the same dimensions as the prism in Figure 4, but with a 200:1 resistivity contrast between the prism and the background, and with a depth of burial equal to

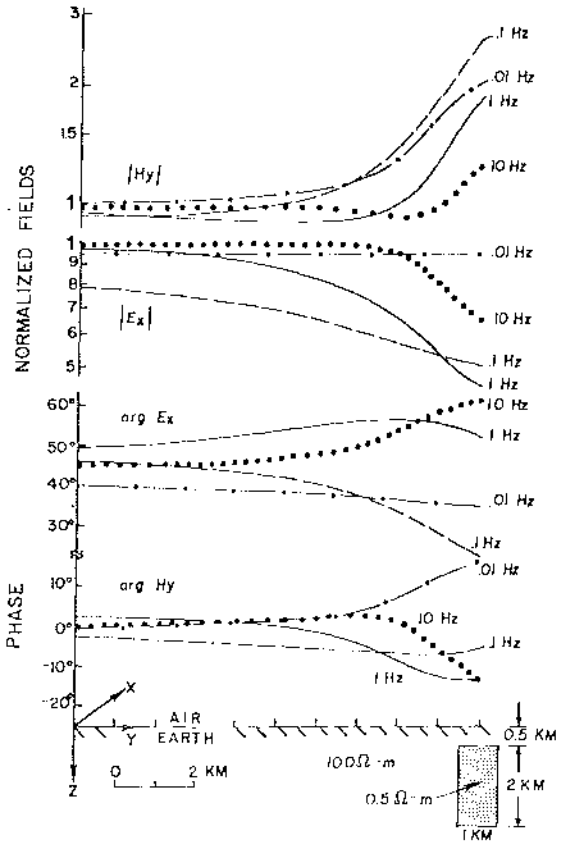

FIG. 6. Spatial variation of the TE mode horizontal field components across a shallow 2-D prism.

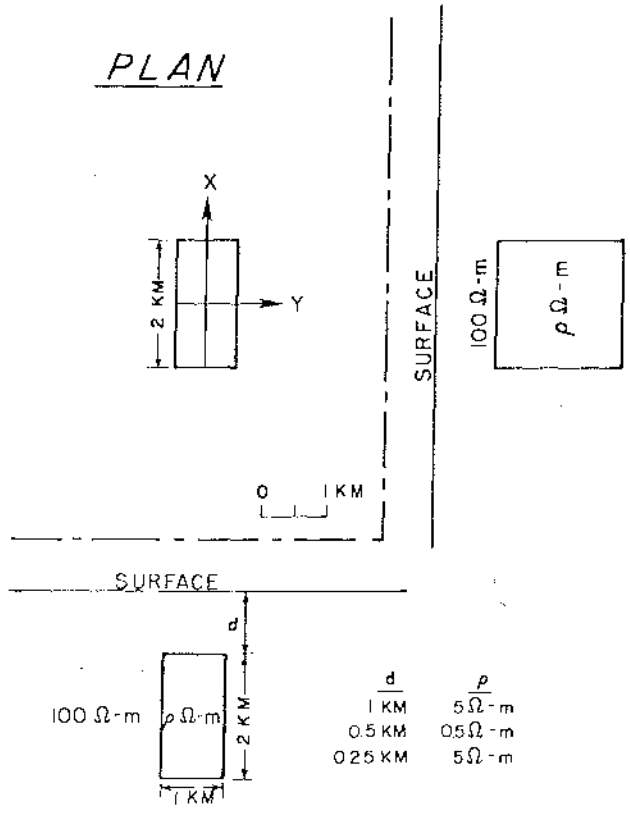

FIG. 7. Plan and section views of a 3-D prism model with length and depth extent equal to twice its width. Modeled depths to the prism's top and corresponding prism resistivities are listed in the table of d and ρ.

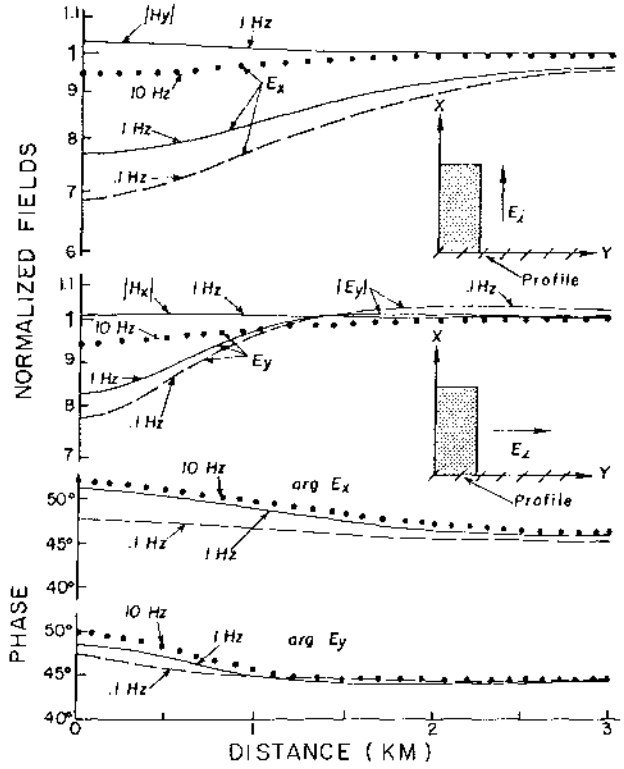

FIG. 8. Spatial variation of the horizontal field components over the prism model of Figure 7, with d = 1 km and ρ = 5 Ω-m. E_i is the incident electric field.

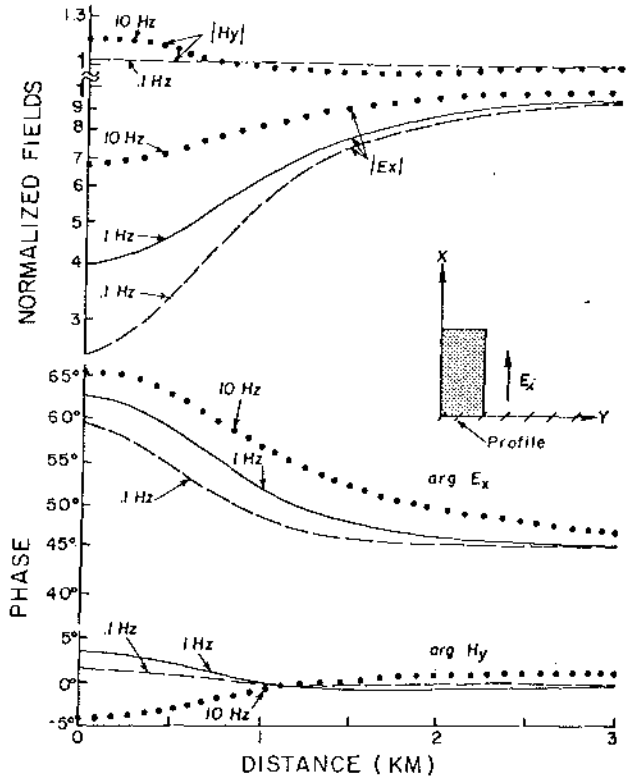

FIG. 9. Spatial variation of the field components E_x and H_y over the prism model of Figure 7, with d = 0.5 km and ρ = 0.5 Ω-m. E_i is the incident electric field.

half the width of the prism. If the conductivity contrast between the prism and the background is increased or the depth of burial is decreased, we expect the spatial variation of the magnetic field to increase because larger secondary currents are induced in the prism, as comparison of Figure 6 with Figure 4 illustrates. At each frequency, the spatial variation of the magnetic field is substantially greater over the shallow, more conductive prism. For example, at 0.1 Hz, the magnitude of the magnetic field varies by approximately a factor of 1.2 over the deep prism, compared to a variation of nearly a factor of three over the shallow, more conductive prism. Neglecting the magnetic field variation would cause discrepancies between MT and T-MT apparent resistivities as large as factors of 1.44 and 9, respectively, over the deep and shallow prisms.

Three-dimensional results

In order to obtain results to compare directly with the 2-D data of Figures 4 and 6, the 3-D prism of Figure 7 was used. The resistivity contrasts and the cross-sections transverse to the long axis of the prism are the same as those of the 2-D models of Figures 4 and 6; the strike-length of the anomalous body is twice its width in each case. Calculations from the integral equation solution at 10, 1, and 0.1 Hz are presented in Figures 8, 9, and 10 along a profile in the symmetry plane transverse to the long axis of the body. Results are presented for incident electric fields polarized

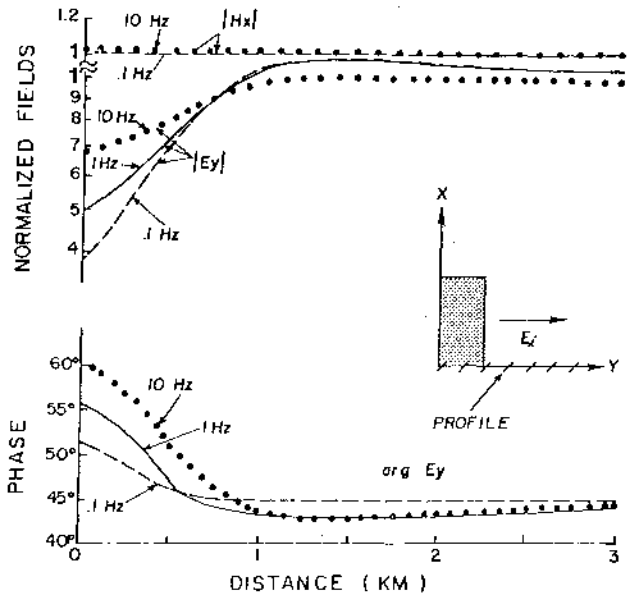

FIG. 10. Spatial variation of the field components E_y and H_x over the prism model of Figure 7, with d = 0.5 km and ρ = 0.5 Ω-m. E_i is the incident electric field.

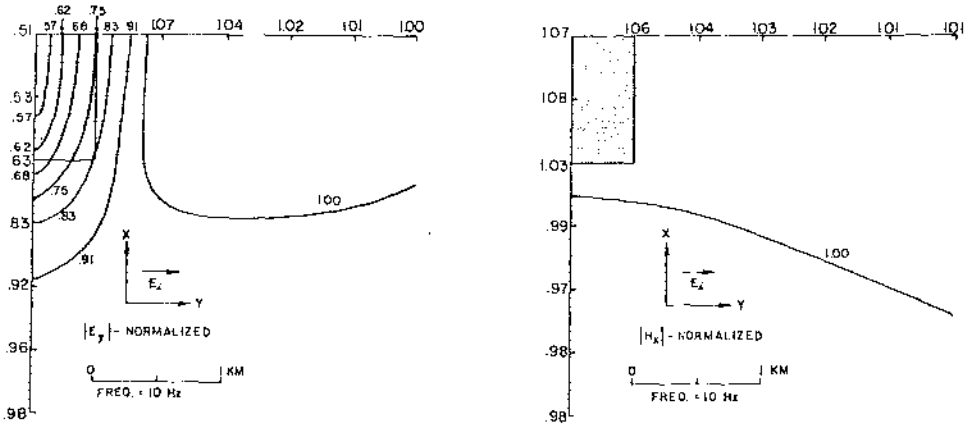

FIG. 11. Plan map of spatial variation of the magnitudes of E_y and H_x over the prism model of Figure 7, with $d = 0.25$ km and $\rho = 5\ \Omega$-m. E_i is the incident electric field. Contour lines represent successive factors of 1.1 variation in magnitude.

parallel to and perpendicular to the long axis of the body. Again, only half of the profile has been plotted because of symmetry.

A comparison of Figure 8 with Figure 4 and of Figures 9 and 10 with Figure 6 shows fundamental differences in behavior of 2-D and 3-D earth models. Over the 3-D prism, calculations at all three frequencies show that spatial variation in the electric field strongly influences the spatial variation of impedance magnitude and phase, particularly at low frequencies. This behavior is observed for both source polarizations and is just the opposite of that encountered in the TE-mode calculations over 2-D prism models. The variation in phase of the horizontal magnetic field is less than two degrees in Figures 8 and 10 and is not plotted. The spatial variation in the horizontal magnetic field is largest for an incident electric field polarized parallel to the long axis of a conductive inhomogeneity. Figure 9 shows that the maximum variation in the magnitude of H_y is less than 15 percent, even for this polarization. Thus T-MT apparent resistivities calculated by ignoring this variation will differ from MT apparent resistivities by no more than 35 percent.

As a conductive inhomogeneity nears the surface, the secondary horizontal magnetic field becomes stronger, because the scattering current in the body is greater. Moreover, the secondary fields associated with this scattering current will be less attenuated during propagation back to the earth's surface. To examine the spatial variation of the total fields over a shallow body, we calculated the response of the 3-D prism of Figure 7, with a depth d of 0.25 km, at 10, 1, and 0.1 Hz. The resistivity contrast is 20:1, coinciding with the contrast used for the 3-D prism calculations presented in Figure 8 where the depth was 1 km. Because of computer storage limitations and crudeness of the approximation made for the scattering current, we were not able to study the spatial behavior of the magnetic field over this prism when buried at depths less than 0.25 km.

Plan maps of the spatial variation of the normalized magnitudes of E_y and H_x and of E_x and H_y at 10 Hz are presented in Figures 11 and 12. The incident electric field for these two figures is oriented transverse to and parallel to the long axis of the prism, respectively. It is apparent from Figures 11 and 12 that the electric field spatial variation is both much larger and more rapid than the spatial variation of the magnetic field. However, the magnetic field does vary by as much as a factor of 1.25 in Figure 12, where the incident

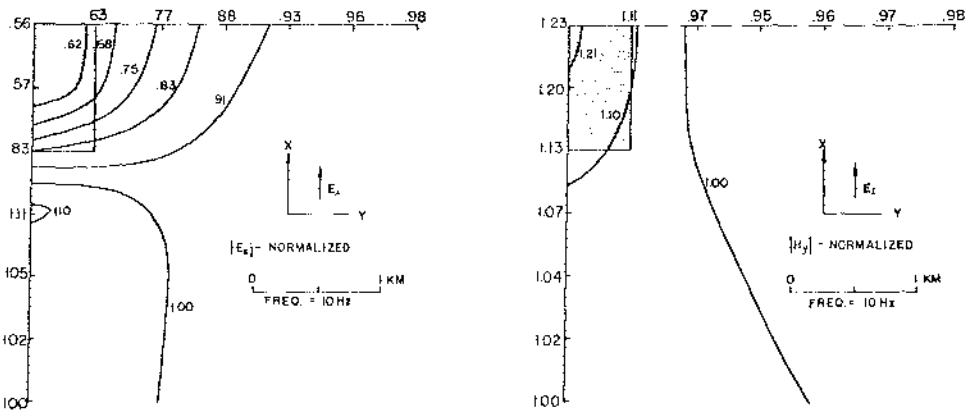

FIG. 12. Plan map of spatial variation of the magnitudes of E_x and H_y over the prism model of Figure 7, with $d = 0.25$ km and $\rho = 5\ \Omega$-m. E_i is the incident electric field. Contour lines represent successive factors of 1.1 variation in magnitude.

electric field is polarized parallel to the long axis of the body. This variation results in at most a 60 percent difference between T-MT and MT apparent resistivity calculations.

Figures 13 and 14 are plots of the spatial variation of the field components E_x and H_y at 10, 1, and 0.1 Hz along profiles in the vertical symmetry planes of the shallow prism, for the incident electric field oriented parallel to the long axis of the prism. These plots again illustrate that the spatial variation in the magnetic field ultimately decreases with decreasing frequency. Below 1 Hz the total variation is less than a factor of 1.1. The spatial variation in the phase of the magnetic field appears significant for this model only at frequencies near 1 Hz. In contrast, the spatial variation in the magnitude of the electric field increases with decreasing frequency toward a dc limiting value. This behavior is caused by electric charge (surface charge) which must be maintained at boundaries between two media of differing conductivity in order to preserve continuity of the normal component of total current density at the interface.

We can derive an expression for the surface charge $\rho_s(\omega)$ at an interface between two media with different electrical constants from the boundary conditions on the normal components of the current density $y\mathbf{E}$ and the displacement vector $\mathbf{D} = \varepsilon\mathbf{E}$. If the permittivity ε is constant, the boundary conditions are (Stratton, 1941)

$$\mathbf{n} \cdot \{y_2\mathbf{E}_2(\omega) - y_1\mathbf{E}_1(\omega)\} = 0 \tag{20}$$

and

$$\mathbf{n} \cdot \varepsilon\{\mathbf{E}_2(\omega) - \mathbf{E}_1(\omega)\} = \rho_s(\omega), \tag{21}$$

where $\mathbf{n}$ is a unit vector normal to the interface directed from medium 1 to medium 2. Let $\mathbf{n} \cdot \mathbf{E}_i(\omega) \equiv E_i^n$. If we solve equation (20) for either E_1^n or E_2^n and substitute the result in equation (21), we get

$$\rho_s(\omega) = \frac{\varepsilon E_2^n(1 - \sigma_2/\sigma_1)}{1 + j\omega\varepsilon/\sigma_1} = \frac{\varepsilon E_1^n(\sigma_1/\sigma_2 - 1)}{1 + j\omega\varepsilon/\sigma_2}, \tag{22}$$

where $E_{1,2}^n = E_p^n(1 + E_{s_{1,2}}^n/E_p^n)$. Note that ignoring displacement currents reduces the denominators in equation (22) to unity but does not cause the charge to vanish.

The primary field $\mathbf{E}_p$ was defined as the field of a plane wave source over a 1-D structure in equations (3), so for normal incidence $\nabla \cdot \mathbf{E}_p$ is zero because $\mathbf{E}_p$ is parallel to all interfaces and no charge is established. Thus $\rho_s(\omega)$ is the divergence of the secondary displacement field $\mathbf{D}_s$. The magnitude of this charge distribution depends on the primary field strength, as does the magnitude of $\mathbf{E}_s$. Equation (22) shows that the surface charge distribution is a function of the normal components of electric field at the interface and of the conductivity contrast, weighted by the permittivity ε. Therefore, ρ_s is minute, although the fields produced by it are not small, because $\nabla \cdot \mathbf{E}_s = \rho_s/\varepsilon$ (Price, 1973). As frequency decreases, induction in the body is negligible, and the ratio E_s^n/E_p^n becomes independent of frequency. Hence, from

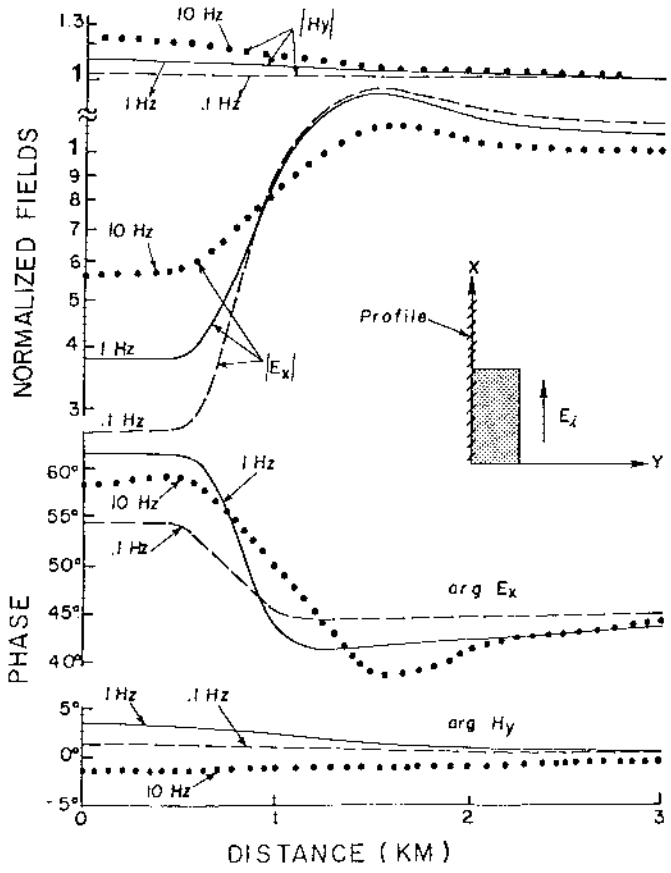

FIG. 13. Spatial variation of the field components E_x and H_y on the longitudinal symmetry axis of the prism of Figure 7, with $d = 0.25$ km and $\rho = 5$ Ω-m. E_i is the incident electric field.

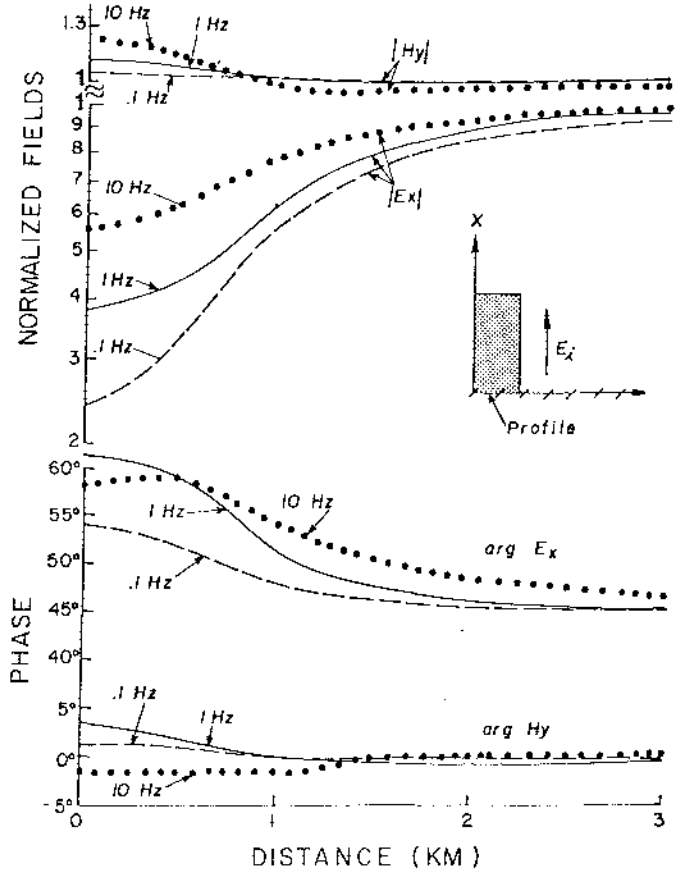

FIG. 14. Spatial variation of the horizontal field components E_x and H_y on the transverse symmetry axis of the prism of Figure 7, with $d = 0.25$ km and $\rho = 5$ Ω-m. E_i is the incident electric field.

equation (22), $\rho_s(\omega)$ approaches a static spatial distribution, its only frequency dependence being that of the primary field.

The different spatial behavior of the electric and magnetic fields can now be explained. The reflection coefficients at the surface of a 1-D earth indicate that the amplitude of $\mathbf{H}_p$ is essentially constant with frequency, while the amplitude of $\mathbf{E}_p$ varies as $\omega^{1/2}$ as $\omega \to 0$. Thus $\mathbf{E}_s$, $\mathbf{H}_s$, and ρ_s, which are caused by the scattering current $y_s\mathbf{E}$, ultimately decrease with decreasing frequency. From equations (2), the total fields comprise the sum of primary and secondary parts, so the total magnetic field at the earth's surface approaches spatial uniformity as frequency decreases. But the total electric field remains distorted by the effects of surface charge as frequency decreases, because both the primary and secondary electric fields vary as $\omega^{1/2}$.

DISCUSSION AND CONCLUSIONS

The difference in spatial behavior between the 2-D TE-mode fields and the corresponding 3-D field components when the incident electric field is parallel to the long axis of these prism models is due primarily to the effects of surface charge. There is no surface charge present for the 2-D TE-mode, because the electric field vector is always aligned parallel to interfaces between regions of differing conductivity. Since there is no component of current flow normal to these interfaces, no charge is established, leaving induction as the only mechanism producing lateral variation in the horizontal field components. For 3-D conductivity inhomogeneities, there will always be a significant component of current density normal to interfaces regardless of incident field polarization. Surface charge effects also are present in the 2-D TM-mode response because current flows transverse to the strike of any conductivity inhomogeneity. Swift (1967) suggested that, in lieu of 3-D modeling capability for complicated structures, modeling selected field data from a 3-D area with a 2-D TM algorithm may yield more accurate conductivity cross-sections than those obtained with a TE algorithm. This notion is supported by comparisons of MT impedance behavior over 2-D and 3-D prism models presented by Ting and Hohmann (1981). Wannamaker (1978) has used 2-D TM-mode modeling to advantage in his attempts to interpret MT data from the Roosevelt Hot Springs KGRA in southwestern Utah, and we suggest that 2-D TM-mode modeling of T-MT data be given priority over TE-mode modeling, until general 3-D interpretational aids are developed.

The spatial variation of the magnetic field over the 2-D models discussed in this paper accounts for a significant percentage of the spatial variation in TE-mode impedance magnitude and phase. In fact, Figures 4 and 6 illustrate that as frequency decreases over the range of inductive response of the 2-D prism models considered here, the spatial variation of the magnetic field becomes the prime indicator of the presence of the inhomogeneity in the TE-mode response. The spatial variation of the magnetic field is less over 3-D conductivity inhomogeneities than it is over 2-D inhomogeneities with the same cross-section. However, the variation may become significant over shallow 3-D bodies at high frequencies, as suggested by Figures 13 and 14. The model calculations suggest that the different spatial behavior of electric and magnetic fields as a function of frequency could be useful for distinguishing between certain 2-D and 3-D inhomogeneities. But obtaining the appropriate measurements would require more work than even a standard MT survey requires.

When the magnetic field varies laterally, T-MT impedance tensors calculated by relating the electric fields at a remote site to magnetic fields at different base sites can differ significantly from each other as well as from the MT impedance tensor at the remote site. Consequently, MT apparent resistivities and phases can, as shown in Figures 3 and 5, differ significantly from their T-MT counterparts. MT interpretation of T-MT data could lead to erroneous conclusions about earth conductivity structure when the magnetic field varies significantly. Thus, numerical modeling programs should calculate T-MT rather than MT responses for comparison with T-MT data. A trivial modification to a 2-D TE-mode algorithm is required at the point where apparent resistivities and phases are calculated to incorporate a base station magnetic field in place of the magnetic field at a remote site. A 3-D algorithm must be modified at the point where the impedance elements, rather than the apparent resistivities and phases, are calculated, because these quantities in general cannot be calculated from simple ratios of orthogonal electric and magnetic field pairs, as in the 2-D problem. A 2-D TM-mode algorithm obviously needs no modification when flat air-earth interfaces are considered.

In any case, neglect of significant response in the magnetic field undoubtedly reduces the resolution of conductivity structure. The calculations presented here suggest that greater loss of information occurs over 2-D structures and elongate 3-D structures than occurs over nearly equidimensional 3-D structures. However, in many applications, speed of T-MT data acquisition may offset this shortcoming, provided the data are properly interpreted.

ACKNOWLEDGMENTS

The authors would like to thank Dr. S. H. Ward for critically reviewing this manuscript. Useful discussions with Phillip Wannamaker are also acknowledged. This work was supported under contract EG-78-C-07-1701 from the Dept. of Energy. One of the authors (J. Stodt) was partially supported by NSF contract no. AER 76-11155 while preparing this report.

REFERENCES

Cagniard, L., 1953, Basic theory of the magnetotelluric method: Geophysics, v. 18, p. 605–635.
d'Erceville, I., and Kunetz, G., 1962, The effect of a fault on the earth's natural electromagnetic field: Geophysics, v. 27, p. 651–665.
Geyer, R. G., 1972, The effects of a dipping contact on the behavior of the electromagnetic field: Geophysics, v. 37, p. 337–350.
Hermance, J. F., 1973, Processing of magnetotelluric data: Phys. Earth and Plan. Int., v. 7, p. 349–364.
Hermance, J. F., and Thayer, R. E., 1975, The telluric-magnetotelluric method: Geophysics, v. 40, p. 664–668.
Hermance, J. F., Thayer, R. E., and Bjornsson, A., 1976, The telluric-magnetotelluric method in the regional assessment of geothermal potential: Proc. 2nd U.N. symp. on the dev. and use of geothermal res., v. 2, p. 1037–1048.
Hughes, W. J., 1974, The polarization of micropulsations and geo-electric structure: Geophys. J. Roy. Astr. Soc., v. 38, p. 95–117.
Jones, F. W., 1973, Induction in laterally non-uniform conductors: theory and numerical models: Phys. Earth and Plan. Int., v. 7, p. 282–293.
Jones, F. W., and Pascoe, L. J., 1972, The perturbation of alternating geomagnetic fields by three-dimensional conductivity inhomogeneities: Geophys. J., v. 27, p. 479–485.
Lines, L. R., and Jones, F. W., 1973a, The perturbation of alternating geomagnetic fields by three-dimensional island structures: Geophys. J. Roy. Astr. Soc., v. 32, p. 133–154.
—— —— 1973b, the perturbation of alternating geomagnetic fields by an island near a coastline: Can. J. Earth Sci., v. 10, p. 510–518.
Price, A. T., 1973, The theory of geomagnetic induction: Phys. Earth and Plan. Int., v. 7, p. 227–233.
Rijo, L., 1977, Modeling of electric and electromagnetic data: Ph.D. thesis, Univ. of Utah.
Stodt, J. A., 1978, Documentation of a finite-element program for solution of geophysical problems governed by the 2-D, scalar Helmholtz equation: Univ. of Utah, program listing and documentation, NSF contr. AER 76-11155.
Stratton, J. A., 1941, Electromagnetic theory: New York, McGraw-Hill Book Co., Inc.
Swift, C. M., Jr., 1967, A magnetotelluric investigation of an electrical conductivity anomaly in the southwestern United States: Ph.D. thesis, MIT.
—— —— 1971, Theoretical magnetotelluric and Turam response from two-dimensional inhomogeneities: Geophysics, v. 36, p. 38–52.

Ting, S. C., and Hohmann, G. W., 1981, Integral equation modeling of three-dimensional magnetotelluric response: Geophysics, v. 46, p. 182–197.
Wannamaker, P., 1978, Magnetotelluric investigations at the Roosevelt Hot Springs KGRA and Mineral Mountains, Utah: Univ. of Utah DOE/DGE Rep. 78-1701.a.6.1.
Weaver, J. T., 1963, The electromagnetic field within a discontinuous conductor with reference to geomagnetic micropulsations near a coastline: Can. J. Phys., v. 41, p. 484–495.
Weidelt, P., 1975, Electromagnetic induction in three-dimensional structures: J. Geophys., v. 41, p. 85–109.
Yungul, S. H., 1966, Telluric sounding—A magnetotelluric method without magnetic measurements: Geophysics, v. 31, p. 185–191.